AN ANALYSIS OF POST-FIRE ACTIVE REFORESTATION USING SENTINEL-2

Miriam Bakija
University of Alberta
Edmonton, Canada
bakija@ualberta.ca

Bailey Kacsmar
University of Alberta
Edmonton, Canada
kacsmar@ualberta.ca

Irene Cheng
University of Alberta
Edmonton, Canada
locheng@ualberta.ca

***Abstract*—Forest fires are becoming increasingly frequent and severe. Identifying appropriate reforestation practices after these fires is essential to support biodiversity and to reduce carbon impact. To aid in informed reforestation decision-making, we identify an approach for using remote sensing to evaluate the relationship between passive regrowth and artificial reforestation by monitoring vegetation regrowth over the first six years after a forest fire. Our novel approach temporally extends existing methods to identify vegetative regeneration zones using clustering on differenced vegetation index images. Our use of remote sensing illustrates that over time, areas of enhanced vegetation regrowth decrease. Additionally, we identify that areas which had high levels of passive regrowth in the first four months post-fire have higher average vegetation density in the burned area five years later, after artificial reforestation has occurred. Together these conclusions indicate the potential for utilizing remote sensing in understanding and developing impactful reforestation strategies that employ both passive and active regeneration.**

***Index Terms*—Forest fires, remote sensing, clustering methods, vegetation index, reforestation.**

I. Introduction

The frequency of forest fires over the past few decades has significantly increased [1]. Fire-affected regions require ongoing and efficient vegetation regrowth to re-establish the forest systems' climate mitigation effect [2]. Fire-affected land becomes reforested through passive regeneration, artificial regeneration, or a combination of the two. Passive regeneration occurs when a variety of plant species and saplings naturally regrow while artificial reforestation employs human efforts to clear the area of burned vegetation and then replant saplings. Artificial reforestation is a lengthy process, often taking many years to complete, and requires significant funding. Therefore, we require techniques to support effective decision-making about when and where to artificially reforest most effectively.

Remote sensing techniques are well suited for understanding post-fire vegetation regrowth in terms of their practicality for frequently and inexpensively monitoring large regions. Recent methodologies employing remote sensing have used machine learning techniques to uncover relationships between post-fire vegetation recovery and environmental factors like vegetation type, time since fire occurred, and elevation [3–6].

While we focus on understanding the relationship between short-term passive regrowth and long-term artificial reforestation with our remote sensing methodology, past works have investigated the differences in artificial versus passive reforestation [7, 8]. Specifically, we use two guiding questions to advance the literature on post-fire reforestation in terms of understanding mixed reforestation techniques over time:

- How can we identify fast-growing regions after artificial reforestation has occurred?
- How do burned areas with high passive regrowth shortly after a fire fair long term regarding vegetation density?

To answer these questions, we examine a burned area following a 2019 forest fire in South Korea. We identify Vegetation Regeneration Zones (VRZs) in the fire-affected region using a clustering algorithm and determine their spatial significance using Getis-Ord Gi* (GOG*) statistics. VRZs are areas where vegetation density is increasing at the highest rates in the fire-affected region and we track and analyze yearly changes in the VRZs to answer our research questions.

Our main contribution is the introduction of our methodology to analyze how vegetation density in a burned region changes under artificial reforestation. Our methodology is designed to provide insight into the relationship between passive regeneration and artificial reforestation, to aid those in charge of reforestation projects in deciding when to prioritize passive regeneration over clearing and replanting, and ultimately in choosing the most carbon-efficient strategies.

II. Methodology

A. Study Area and Data Collection

Our data is from the Sentinel-2 mission, which consists of two satellites that use multispectral sensors to capture 13 bands of light spanning the visible to the infrared. The sensors have a spatial resolution of up to 10 m for certain bands and a revisit time of five days. We use data from the Sentinel-2 A and B satellites collected via the Google Earth Engine API [9].

We examine the aftermath of the April 2019 forest fire in Okgye town, Gangneung city, South Korea, which burned around 7 km^2 of mainly pine forest. We examine the change in the region over six yearly time stamps. Artificial reforestation began in the region in September 2019, and was an ongoing process, with reports of community replanting efforts in 2022 and 2023 [10, 11]. Data from the region includes the following dates: March 26th 2019, right before the fire; April 20th 2019, right after; and each subsequent August from 2019 to 2025. August was chosen to evaluate results to avoid seasonal

(a) Hand drawn from Kim et al. (2021)

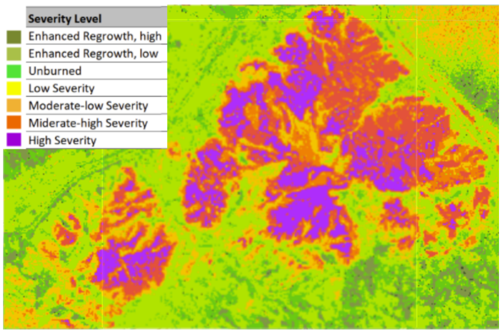

(b) dNBR fire severity map using USGS thresholds

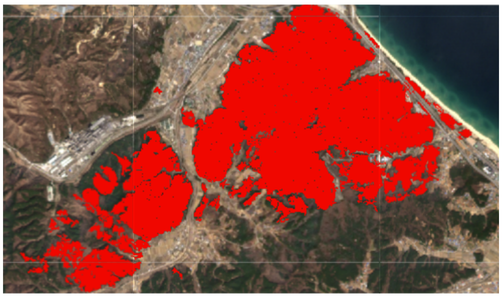

(c) Our final derived burned mask using spectral indices

Fig. 1: Comparison of burned regions derived using three different methods (hand drawn, dNBR only, and our method).

distortion. Images were visually evaluated to find the first cloudless image closest to August 8th of each year.

B. *Deriving the Burned Region*

We advance prior efforts to examine and derive burned regions. In 2021, Kim et al. derived a hand drawn burned region of the area, which is illustrated in the RGB satellite image of the region one week post-fire in Figure 1a [12]. To increase the generalizability of such illustrations we developed a method to estimate burned regions using spectral indices.

The Normalized Burn Ratio (NBR) [13] measures burn severity remotely. The differenced NBR (dNBR) compares NBR values directly before and after the fire as shown for the region of interest in Figure 1b. We create a mask of only pixels with a dNBR value of 0.1 or greater using the US Geological Survey (USGS) threshold chart for burned regions [14]. After masking, two additional problems remain. First, the ocean, seen in the top-right of the images in Figure 1, was classified as a low-severity burn, which is intuitively false. Therefore, we used an additional spectral index, the Normalized Difference Water Index (NDWI) [15] to create an additional mask to remove all pixels with NDWI values of 0.3 or higher, to remove the body of water. Finally, we applied a morphological operation to remove any remaining pixel clusters with a total area less than 100 pixels. After applying all of our components, our final burned mask was derived and illustrated in Figure 1c. The final burned mask bears similarities to the original burned region derived by Kim et al. (2021) [12]. However, some notable differences appear. For example, our spectral index-derived region has numerous distinct patches, whereas the original is limited to just two contiguous regions. We discuss later how these differences may affect the final VRZs in Section III-A.

C. *Vegetation Indices*

Vegetation Indices (VIs) are deployed to estimate vegetation density and health in a region. We employ three VIs with standardized formulas that use Near-Infrared and Red wavelengths as inputs that have shown to be useful for monitoring post-fire vegetation regrowth [16, 12]. Specifically, we use the Normalized Difference Vegetation Index (NDVI), the Soil Adjusted Vegetation Index (SAVI), and the Enhanced Vegetation Index 2 (EVI) [17, 18]. SAVI [18] is an adaptation of the NDVI formula that adds a soil-adjustment coefficient to correct for variations in soil color and saturation while EVI [17] extends the NDVI formula by adding a soil-adjustment coefficient and an atmospheric correction factor to account for atmospheric effects such as light scattering. Using three different VIs helps account for any potential distortion from a single VI and provides high-confidence estimates of vegetation density. Coefficients were selected by matching values to those reported by Kim et al. (2021) [12] to facilitate comparison of results.

D. *Creating Vegetative Regeneration Zones*

Creating VRZs consists of first mapping the change in VI between the state directly post-fire in 2019 and each year of interest to create differenced images. To identify and separate regions with high confidence that vegetation regeneration is occurring, we use a clustering algorithm. Each of the differenced images was flattened into a single dimension and fed into a Clustering Large Applications (CLARA) algorithm. CLARA is an extension of the k-medoids clustering method that creates k clusters by minimizing the average Euclidean distance to a central point within each cluster. Seven clusters were selected to minimize the Davies-Bouldin Index [19]. One limitation of this method is that, by setting thresholds, spatial information is lost when clustering. We address this later in the results section when discussing the spatial autocorrelation significance analysis using the GOG* statistic [20]. Finally, after the clustering results are obtained for each VI in a given year, the first cluster, that is, the one with the greatest positive change in VI, is selected. The first clusters from each VI are overlapped to create the final VRZ for a given year. We include

(a) Non-clustered dNDVI results

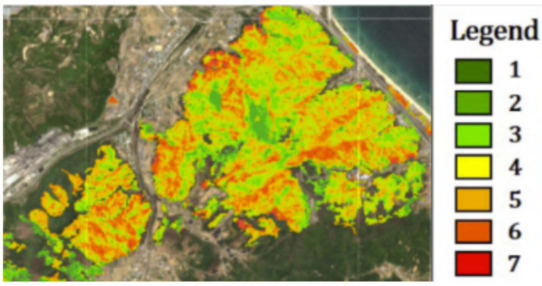

(b) Our clustered dNDVI results

Fig. 2: Differenced dNDVI example over four months.

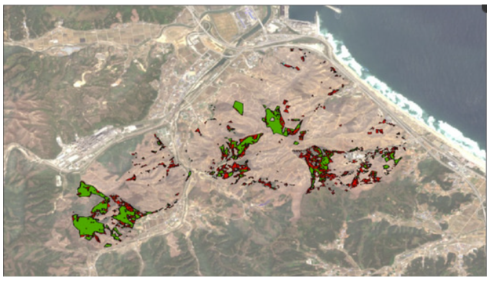

(a) Kim et al. (2021)'s post-fire VRZ

(b) Our post-fire VRZ

Fig. 3: A comparison of the resulting derived 2019 vegetative regeneration zones for the four months following the fire.

an example of the results of clustering in Figure 2b, which is the transformation of Figure 2a after clustering.

III. Results

A. Baseline Comparison Results

To begin, we compare our derived VRZ, indicated by the bright green area in Figure 3b to that derived by Kim et al. 2021 shown in Figure 3a for the four months following the 2019 fire. While the visible overlap is apparent, our VRZ represents only 6.7% of the total area, compared to 12.3% as derived by Kim et al. in 2021. We surmise the main cause of this discrepancy is the difference in derived burned areas. For example, our map did not label as much of the southwest corner of the region as being burned as was labeled by Kim et al. (2021) [12]. Consequently, a larger portion of their VRZ was located in the southwest corner. We propose that the method used by Kim et al. (2021) [12] for identifying the fire-burned region may lead to inaccuracies, falsely labeling unburned areas as being in the VRZ.

VRZ Percentage in the Region					
		Spatial Sig.		Avg. z-score	
Year	Total Area	dEVI	dNDVI	dEVI	dNDVI
2019	6.7%	80.8%	69.4%	1.893	1.764
2020	3.1%	95.5%	75.8%	1.837	1.709
2021	3.8%	86.1%	80.7%	1.879	1.756
2022	5.0%	3.9%	0%	1.377	1.176
2023	6.6%	18.2%	2.8%	1.498	1.419
2024	7.8%	15.9%	4.3%	1.507	1.451
2025	4.3%	1.2%	0%	1.442	1.209

TABLE I: Calculated statistics for VRZs in the region over the years of 2019-2025 for total area and spatial significance.

B. Vegetative Regeneration Zones

Next, we investigate how VRZs evolved over the six years following the fire. We repeated our process for identifying VRZs by taking the difference in VIs between right after the fire in April 2019 and each subsequent August. Our hypothesis was that our VRZs would shift from identifying regions where passive regeneration was occurring to areas that were actively being reforested. However, our results indicate that VRZs decrease in both size and spatial significance over time.

As shown in Table I, we find the size of the total VRZ as a percent of the total burned area ranges from 3.1% to 7.8%, with no consistent trend over time. Notably, none of the VRZs match or exceed the 12% of the total burned area of the VRZ found by Kim et al. (2021) [12]. Even when using fewer clusters (five and six), we still obtained similarly small VRZs. The small size of these zones suggests that this method only identifies areas with high confidence for high regrowth levels. Additionally, we visually observed that compared to the 2019 VRZ, subsequent VRZs are slightly more scattered and contain fewer large contiguous areas.

C. Significance Testing

In terms of how the spatial significance of our VRZs changed over time we used the global GOG* statistic, a global spatial autocorrelation statistic used for hotspot analysis, to get z-scores for each pixel in an image. High z-scores indicate that the pixel and its neighbors have values above average, suggesting a hot spot. For our analysis, we used a spatial weight kernel of size $5x5$, and a one-tailed p-value < 0.05, corresponding to a z-score of 1.645 or greater.

We calculated the GOG* z-score for each yearly VRZ. We performed hotspot analysis of the corresponding years' dNDVI and dEVI maps. dSAVI was skipped because SAVI's

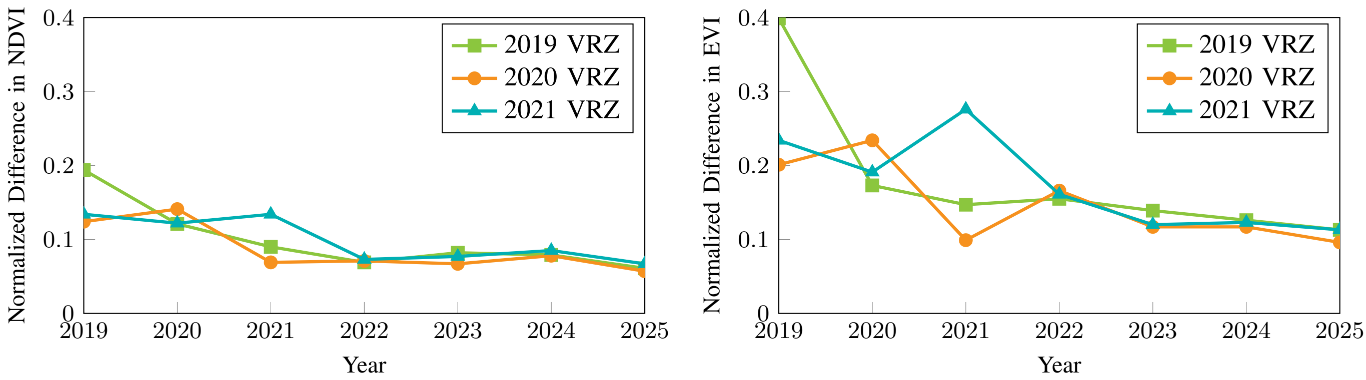

(a) Difference in NDVI

(b) Difference in EVI

Fig. 4: Normalized difference average VIs within and outside of VRZs 2019-2021

formula extends the NDVI distribution and thus yields identical GOG*~~GGO*~~ statistics to dNDVI. In Table I, we see that for both dEVI and dNDVI, the average z-score generally decreases over time, indicating that VRZs are becoming less spatially significant.

We observe in the spatial significance columns of Table I a sharp decrease in percent of significant area in VRZ for both dNDVI and dEVI from 2022 onward. While this is due, in part, to the significance level we chose, there is also a noticeable decrease in average z-scores from 2021 to 2022, unaffected by the significance level. Our methodology alone cannot explain this jump without more detailed ground-truth artificial reforestation to compare against. However, the decrease in spatial significance indicates that the average vegetation distribution in the area is becoming more uniform, making hotspot identification more difficult. Intuitively, the average vegetation density would become more uniform under active reforestation because areas are manually cleared and replanted, leaving less room for environmental factors to create region-wide variations, unlike in passive regrowth.

D. Short-term VRZs in the Long Term

We compare the average VIs inside and outside the VRZs in the burned zone over time to investigate whether VRZs identified in the short term (0-2 years post-fire) had higher vegetation density in the long run than the rest of the burned region. Higher vegetation density several years post-fire could suggest that these areas had saplings that grew than those in areas with low vegetation density.

We investigate 2019-2021's VRZs, chosen based on our spatial significance findings, and illustrate our results in Figure 4. Note that SAVI was once again omitted because it produced identical results to NDVI. The y-axis shows the differences in normalized VI between inside and outside the VRZ for a given year. We see the difference peaks for both EVI and NDVI in 2019. This corresponds to our results from the previous section, which found the highest spatial significance for the 2019 VRZ. The difference decreases over time but remains positive, plateauing around 2022 for each VRZ. Again, we observe a unique shift in 2022, though we are not equipped to explain it with our current information. By 2025, the average NDVI value within the early-identified VRZs was 6% higher, and for EVI, it was 10% higher. This, in and of itself, is a notable finding. Using the existing methodology, we can identify burned regions that will have higher long-term vegetation density, even under artificial reforestation. We propose two possible explanations for this result. First, environmental characteristics such as elevation and burn severity that affect the speed of passive regeneration may have similar positive effects on long-term artificial reforestation vegetation density. Another possibility is that saplings that began growing before artificial reforestation began were avoided in the artificial clearing process, giving them a head start on the rest of the region. Ultimately, under either explanation, our methodology's ability to predict long-term vegetation recovery can assist in choosing optimal artificial reforestation practices, saving money and reducing carbon emissions.

IV. Conclusion

In this work, we demonstrated a new methodology for using remote sensing for analyzing post-fire vegetation changes under passive regeneration and active reforestation. Our results find that under artificial reforestation, it becomes harder to identify spatially significant regions of fast-growing vegetation, suggesting that ultimately the region's vegetation density becomes more homogeneous under artificial reforestation. Additionally, our method successfully predicts long-term vegetation recovery and showed that ~~while~~ areas with good short-term passive regeneration have higher long-term vegetation density. Future work can investigate whether these results generalize to areas beyond our region of interest. Moreover, future work can build upon our insights into the relationship between artificial reforestation and passive regeneration with access to higher detail ground-truth data on artificial reforestation. Knowledge of more precise location with in the region that are the targets for replanting efforts would allow future projects to provide more in depth explanations into why early identified VRZs perform better in the long run. In the interim, our method can still be used to assist in choosing how to utilize artificial reforestation practices in economic ways while still mitigating carbon emissions.

References

[1] M. Flannigan, A. S. Cantin, W. J. De Groot, M. Wotton, A. Newbery, and L. M. Gowman, “Global wildland fire season severity in the 21st century,” Forest Ecology and Management, vol. 294, pp. 54–61, 2013.

[2] L. E. Nave, B. F. Walters, K. Hofmeister, C. H. Perry, U. Mishra, G. M. Domke, and C. Swanston, “The role of reforestation in carbon sequestration,” New Forests, vol. 50, no. 1, pp. 115–137, 2019.

[3] B. Jiang, W. Chen, Y. Wu, and Z. Gao, “Monitoring vegetation restoration after wildfires in typical boreal forests based on multi-source remote sensing data,” in 2024 IEEE International Geoscience and Remote Sensing Symposium (IGARSS). IEEE, 2024, pp. 581–584.

[4] S. Gülci and M. Wing, “Evaluating forest fire severity and vegetative recovery using sentinel imagery and spectral indices in a cloud-based environment,” Advances in Space Research, 2025.

[5] D. L. Lacouture, E. N. Broadbent, and R. M. Crandall, “Detecting vegetation recovery after fire in a fire-frequented habitat using normalized difference vegetation index (NDVI),” Forests, vol. 11, no. 7, p. 749, 2020.

[6] P. Oikonomou, V. Karathanassi, V. Andronis, and I. Papoutsis, “Assessing and forecasting natural regeneration in Mediterranean landscapes after wildfires,” Remote Sensing, vol. 17, no. 5, p. 897, 2025.

[7] C. Gerlein-Safdi, G. Keppel-Aleks, F. Wang, S. Frolking, and D. L. Mauzerall, “Satellite monitoring of natural reforestation efforts in China’s drylands,” One Earth, vol. 2, no. 1, pp. 98–108, 2020.

[8] W. Chen, K. Moriya, T. Sakai, and C. Cao, “Monitoring of post-fire forest recovery under different restoration treatments based on time-series ALOS/PALSAR data,” in 2016 IEEE International Geoscience and Remote Sensing Symposium (IGARSS), 2016, pp. 1749–1752.

[9] European Space Agency (ESA) / Copernicus, “Sentinel-2 msi: Multispectral instrument, level-2a (harmonized),” Google Earth Engine Data Catalog, 2025. [Online]. Available: developers.google.com/earth-engine/datasets/catalog/COPERNICUS_S2_SR_HARMONIZED

[10] G.-W. Kim, “소나무숲만들려다산다태웠다,” https://h21.hani.co.kr/arti/society/environment/52152.html, 2022-6-21, [Online] Accessed: 2025-12-07.

[11] J.-D. Lee, “제78회식목일기념, 시민과함께하는나무심기행사[출처] 중앙뉴스미디어,” https://www.ja-media.kr/news/article.html?no=520361, 2023-3-31, [Online] Accessed: 2025-12-07.

[12] Y. Kim, M.-H. Jeong, M. Youm, J. Kim, and J. Kim, “Recovery of forest vegetation in a burnt area in the Republic of Korea: A perspective based on Sentinel-2 data,” Applied Sciences, vol. 11, no. 6, p. 2570, 2021.

[13] A. E. Cocke, P. Z. Fulé, and J. E. Crouse, “Comparison of burn severity assessments using differenced normalized burn ratio and ground data,” International Journal of Wildland Fire, vol. 14, no. 2, pp. 189–198, 2005.

[14] D. C. Lutes, R. E. Keane, J. F. Caratti, C. H. Key, N. C. Benson, S. Sutherland, and L. J. Gangi, “Firemon: Fire effects monitoring and inventory system,” General Technical Report RMRS-GTR-164. Fort Collins, CO: US Department of Agriculture, Forest Service, Rocky Mountain Research Station. 1 CD., vol. 164, 2006.

[15] B.-C. Gao, “NDWI—a normalized difference water index for remote sensing of vegetation liquid water from space,” Remote Sensing of Environment, vol. 58, no. 3, pp. 257–266, 1996.

[16] S. Rahman, H.-C. Chang, C. Magill, K. Tomkins, and W. Hehir, “Spatio-temporal assessment of fire severity and vegetation recovery utilising Sentinel-2 imagery in New South Wales, Australia,” in 2019 IEEE International Geoscience and Remote Sensing Symposium (IGARSS), 2019, pp. 9960–9963.

[17] Z. Jiang, A. R. Huete, K. Didan, and T. Miura, “Development of a two-band enhanced vegetation index without a blue band,” Remote Sensing of Environment, vol. 112, no. 10, pp. 3833–3845, 2008.

[18] A. R. Huete, “A soil-adjusted vegetation index (SAVI),” Remote Sensing of Environment, vol. 25, no. 3, pp. 295–309, 1988.

[19] D. L. Davies and D. W. Bouldin, “A cluster separation measure,” IEEE Transactions on Pattern Analysis and Machine Intelligence, no. 2, pp. 224–227, 2009.

[20] A. Getis and J. K. Ord, “The analysis of spatial association by use of distance statistics,” Geographical Analysis, vol. 24, no. 3, pp. 189–206, 1992.